Bull. Chem. Soc. Ethiop. **2022**, 36(1), 209-222.
DOI: https://dx.doi.org/10.4314/bcse.v36i1.17

ISSN 1011-3924
Printed in Ethiopia
Online ISSN 1726-801X

EFFECT OF STABILIZER ON OPTICAL BAND GAP OF ZnO AND THEIR PERFORMANCE IN DYE-SENSITIZED SOLAR CELLS

A. Kalam[1,2*], S.A.S. Allami[1], A.G. Al-Sehemi[1,2], M.A. Assiri[1] and P. Yadav[3]

[1]Department of Chemistry, Faculty of Science, King Khalid University, P.O. Box 9004, Abha 61413, Saudi Arabia
[2]Research Center for Advanced Materials Science (RCAMS), King Khalid University, P.O. Box 9004, Abha 61413, Saudi Arabia
[3]Department of Solar Energy, School of Technology, Pandit Deendayal Petroleum University, Gujarat, India

(Received December 7, 2021; Revised March 9, 2022; Accepted March 9, 2022)

ABSTRACT. In dye-sensitized solar cells, transparent metal oxide working electrodes play a vital role in defining the power conversion efficiency. It was found that the size of nanoparticles influences the electrical, optical properties of these electrodes. Herein, we describe the synthesis of ZnO with zinc acetate dihydrate and different stabilizers (diethylamine and triethylamine) by using a modified solvothermal process. The obtained materials were characterized by XRD, SEM, EDX, TEM, HRTEM, UV-visible, FTIR, and Raman methods. The crystallite sizes for ZnO-1 and ZnO-2 samples were indexed as 39.0 and 40.5 nm for the highest peak intensity with diethylamine and triethylamine stabilizer, respectively. We examine the effect of stabilizers on the morphology, optical band gap, and photovoltaic performance of the prepared ZnO. We found that ZnO prepared using diethylamine stabilizer exhibiting significant efficiency of 1.45%, open-circuit voltage 0.454 V, short-circuit current density 2.128 mA/cm^2, and 0.66 fill factor were achieved under 44 mW/cm^2 illumination powers with dye-3.

KEY WORDS: Dye-sensitized solar cells, ZnO, Band gap, Photovoltaic performance

INTRODUCTION

Semiconductor nanoparticles have received much attention from researchers in multidisciplinary fields such as nanoscale electronic devices, solar cells, light-emitting nanodevices due to exceptional advantages like the optical band gap and size. The optical band gap is directly related to the photo ability of the material, and nanoscale size can impact the physicochemical properties of a material yielding unique properties owing to their large surface area or quantum size effect, such as the optical properties.

Among semiconductor materials, zinc oxide semiconductor (ZnO) has many specific properties such as a wide band gap in the near-UV spectral region with band gap energy of 3.37 eV at room temperature (R.T.), good transparency, considerable free-exciton binding energy (60 meV), high electron mobility (200-1000 cm^2 V^{-1} s^{-1}) and strong room-temperature luminescence as compared to TiO_2 nanomaterials. The wide band gap and considerable excitonic binding energy have highly valued zinc oxide in industrial and scientific circles [1].

Lately, ZnO has become a topic to study for applications such as solar cells [2], memory devices [3], sensors [4], concrete [5], etc. One-dimensional nanostructures seem like an attractive research topic for their great features and applications in nanodevices in the last few years. ZnO's bandgap energy and conduction band are analogous to the anatase TiO_2 materials (3.17–3.28 eV); therefore, it is an alternate working electrode for dye-sensitized solar cell (DSSC) applications [6-9]. But the conversion efficiency confirmed by ZnO is lower than TiO_2 materials based DSSC in which maximum efficiency reached ~13% is achieved [10]. The device performance of ZnO-based DSSC can be improved by setting its morphology, surface area, and size. Several

*Corresponding author. E-mail: abul_k33@yahoo.com

preparation methods have been defined in the literature for preparation of ZnO nanostructures like sol-gel method [11], laser ablation [12], green synthesis [13], co-precipitation [14], electrophoretic deposition [15], sonochemical method [16], hydrothermal method [17], and solvothermal processes [18]. The ordered nanowire DSSC was presented that be very efficient for the excitonic photovoltaic devices [19]. The atomic layer deposition was used to coat arrays of ZnO nanowires with thin shells of amorphous Al_2O_3 or anatase TiO_2 [20]. The dendritic ZnO nanowires were reported with efficiencies of about 0.5% by using the chemical vapor deposition method (CVD) [21-22]. The ZnO nano-flower was prepared through a hydrothermal method and showed an efficiency of up to 1.9% [23]. The ZnO prepared by the solvothermal method exhibited ~2.6% of PCE in DSSC [24]. Remarkably, the hierarchically assembled ZnO nanostructure in a DSSC fabrication gave a high-efficiency reach of ~7.5 [25]. Hence, it is important to synthesize the ZnO nanoparticles with desired crystal structures and controlled particle size.

In the present work, we present a simple, economical, and effective modified solvothermal method to synthesize ZnO nanoparticles using zinc acetate precursor with diethylamine and triethylamine as a stabilizer. The effect of diethylamine and triethylamine on ZnO nanoparticles morphology and optical property will be discussed. In addition, we also discussed the efficiency of ZnO nanoparticles toward dye-sensitized solar cells (DSSCs). In continuation of our previous work, we used 2-cyano-N′-[(2-hydroxynaphthalene-1-yl)methylene]acetohydrazide (CHMA; dye-1), 2-cyano-N′-[(4-dimethylamino)benzylidene]acetohydrazide (CDBA; dye-2) and 2-cyano-N'-[(anthracene-9-yl)methylene]-acetohydrazide (AMCH; dye-3) dyes for this work [26].

EXPERIMENTAL

Synthesis of zinc oxide nanoparticle (ZnO-1)

The standard synthetic procedure to prepare ZnO was as follows: 25 mL of zinc acetate (0.2 N) solution was mixed with 5 mL of diethylamine (drop-wise) in a round bottom flask and stirred at least 30 min. 25 mL of ethanol was added to make the azeotropic mixture and heated at a temperature of 80 °C for 12 h under vigorous stirring, producing white precipitate. The centrifugation was used to separate the precipitate, washed with distilled water and acetone. The residue was heated in an oven at 100 °C for overnight.

Synthesis of zinc oxide nanoparticle (ZnO-2)

Follow the same procedure as mentioned above for ZnO-1, but we used triethylamine instead of diethylamine in the present case.

Preparation of dye

In continuation of our previous work, we prepared and used 2-cyano-N′-[(2-hydroxy naphthalene-1-yl)methylene]acetohydrazide (CHMA; dye-1), 2-cyano-N′-[(4-dimethylamino)benzylidene]-acetohydrazide (CDBA; dye-2) and 2-cyano-N'-[(anthracene-9-yl)methylene]-acetohydrazide (AMCH; dye-3) dyes for this work [26].

Preparation of zinc oxide working electrode and platinum counter electrode by doctor blade method

The as-prepared ZnO was blended with a small volume of acetylacetone, distilled water, and triton X-100 in a conical flask and stirred overnight at 350 rpm to get a colloidal suspension. The paste preparation was done in ambient air at room temperature. An evaporator concentrated the contents in the dispersion at 40 °C. The ultra-sonication was performed for 30 min to homogenize ZnO

paste. The glass substrates were cut to 2 cm x 2 cm and washed ultrasonically in ethanol for 20 min. Additionally, using the doctor blade method, the ZnO pastes were extended on conducting surface of the glass substrate and became dry in the open air to prepare the working electrode. The film was heated at 400 °C for 30 min in the high-temperature furnace. The working electrodes dip in CHMA, CDBA, and AMCH solution for 24 h and are washed with ethanol to eradicate excess dyes from the film's surface. The doctor blade method prepared the platinum counter electrodes and annealed them at 400 °C for 30 min.

Assembling of DSSC

The Pt-coated substrate was generally employed on top of the ZnO-coated substrate and made a sandwich-type device. Therefore, the conductive side of the counter electrode faced the dye-coated ZnO layer. The electrolyte solution (Iodolyte HI-30, iodide/tri-iodide redox couple) was filled in between the working electrode and the counter electrodes, and the complete solar cells were assembled. The conducting side of both electrodes was painted using silver paste and fixed the copper wire used Araldite for getting electrical contact.

Materials characterization and measurement

Different techniques were utilized for the analysis of photoanode, such as X-ray diffractometer (XRD) (Shimadzu Lab X-6000) with Cu-Kα radiation (λ = 1.5406 Å). The samples peaks were observed at room temperature in the range of 2θ from 20º to 80º. The scanning electron microscopy (JSM 6360 SEM/EDX) was employed to study the surface morphologies of the photoanode. The energy dispersive spectroscopy (EDX) is usually fixed with a scanning electron microscope to analyze the elements present in the sample. The JEOL 2100F transmission electron microscopy (TEM) and high-resolution transmission electron microscopy (HR-TEM), operating at 200 kV, were employed to study the photoanode's grain size and morphology. We used PG UV-Vis double-beam spectrophotometer to examine the absorption spectra in the wavelength ranging from 250-to 700 nm. FTIR spectra were examined on a JASCO 460 plus FTIR spectrometer using the KBr pellet technique at room temperature. Raman spectroscopy (XDR, Thermo Fisher Scientific Inc.) was used to find out the vibrational modes of ZnO at an excitation of 532 nm. Keithley 2400 source meters were used to measure the fabricated device's current density-voltage (J-V) at 44 mW cm^{-2} AM 1.5 G of solar spectrum illumination.

RESULTS AND DISCUSSION

Powder X-ray diffraction (XRD) analysis

Figure 1 shows the X-ray diffraction patterns of the samples (ZnO-1 and ZnO-2), which also confirmed the purity of the samples. Our results exhibit sharp and strong reflections, which could be indexed as a pure wurtzite phase of ZnO nanoparticles with a hexagonal structure. The ZnO nanoparticles planes with Miller indices (hkl) values of (100), (002), (101), (102), (110), (103), (200) (112), (201), (004) and (202) for a series of characteristic peaks centered almost 2θ = 31.6°, 34.3°, 36.1°, 47.4°, 56.4°, 62.4°, 66.2°, 67.8°, 69.0°, 72.4°, and 76.8° can be agreed very well with the standard X-ray diffraction pattern of monophasic ZnO nanoparticles (JCPDS card no. 36-1451 [27]. The highest peak intensity is observed with triethylamine than that of diethylamine, which could be due to a better crystalline structure. This preferred orientation (101) is achieved because of covering of progress of certain crystal planes and stimulating the progress of the 101 planes by stabilizers. Miller indices (hkl) and crystallite size (d) of the samples were played a meaningful role to conclude the electrical properties, which can be calculated from the most intense peak signal (101) by applying the Debye–Scherrer formula, $d = 0.9\ \lambda/\beta \cos\theta$. Here, λ

represents the wavelength of X-ray (Cu K_α = 0.154 nm), d represents the size of crystallite (nm), β represents the full width at half maximum (FWHM) of prominent intense peak measured in radians, and θ is the peak angle.

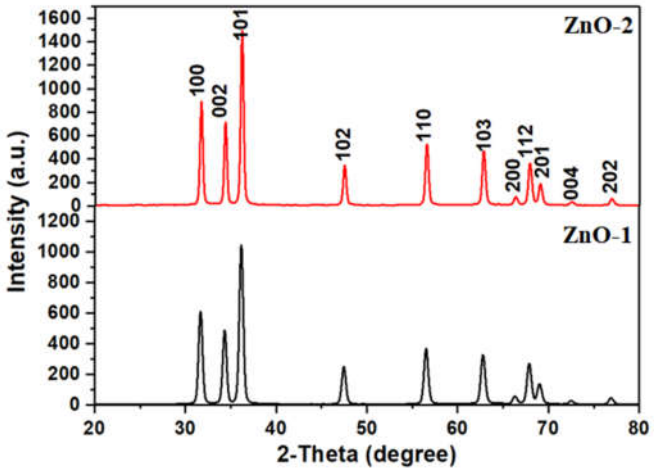

Figure 1. X-ray diffraction pattern of ZnO-1 and ZnO-2 nanoparticles.

Scanning electron microscopy (SEM)

Figure 2 shows the SEM images of ZnO-1 and ZnO-2 nanoparticles formed using diethylamine and triethylamine as stabilizers. The SEM image of ZnO-1 clearly showed a hexagonal crystal structure with a porous texture, whereas the sample ZnO-2 shows nearly spherical particles with low agglomeration. The SEM investigation exhibits that both (diethylamine and triethylamine) have a very significant role in finding the porous hexagonal and spherical morphologies of the ZnO nanoparticles. Yoshida *et al.* [28] have been reported that porous ZnO materials boosted the dye loading and PCE values.

The compositions of nanoparticles in the samples (ZnO-1 and ZnO-2) were determined by EDX analysis (Figure 2), which confirms the presence of Zn and O. Thus, it is also established from EDX analysis that ZnO nanoparticles were formed without any impurities.

Transmission electron microscopy (TEM)

TEM studies were also carried out on ZnO nanoparticles to investigate grain size, morphology, and size distribution. The relevant TEM micrographs are depicted in Figure 3 to conform almost hexagonal for ZnO-1 and spherical for ZnO-2 and uniform as observed by SEM studies. The average particle sizes of ZnO-1 and ZnO-2 samples are in the range of 255 nm to 15.5 nm, respectively, which revealed that by using triethylamine, the grain size decreases from 255 nm to 15.5 nm. The high-resolution transmission electron microscope (HRTEM) shows the spacing between the successive planes of 0.272 nm and 0.252 nm, matching the (101) reflection of pure ZnO nanoparticles. The fringe in the TEM image is linked to a transmitted wave exiting a crystal and a diffracted wave from one lattice plane of the crystal.

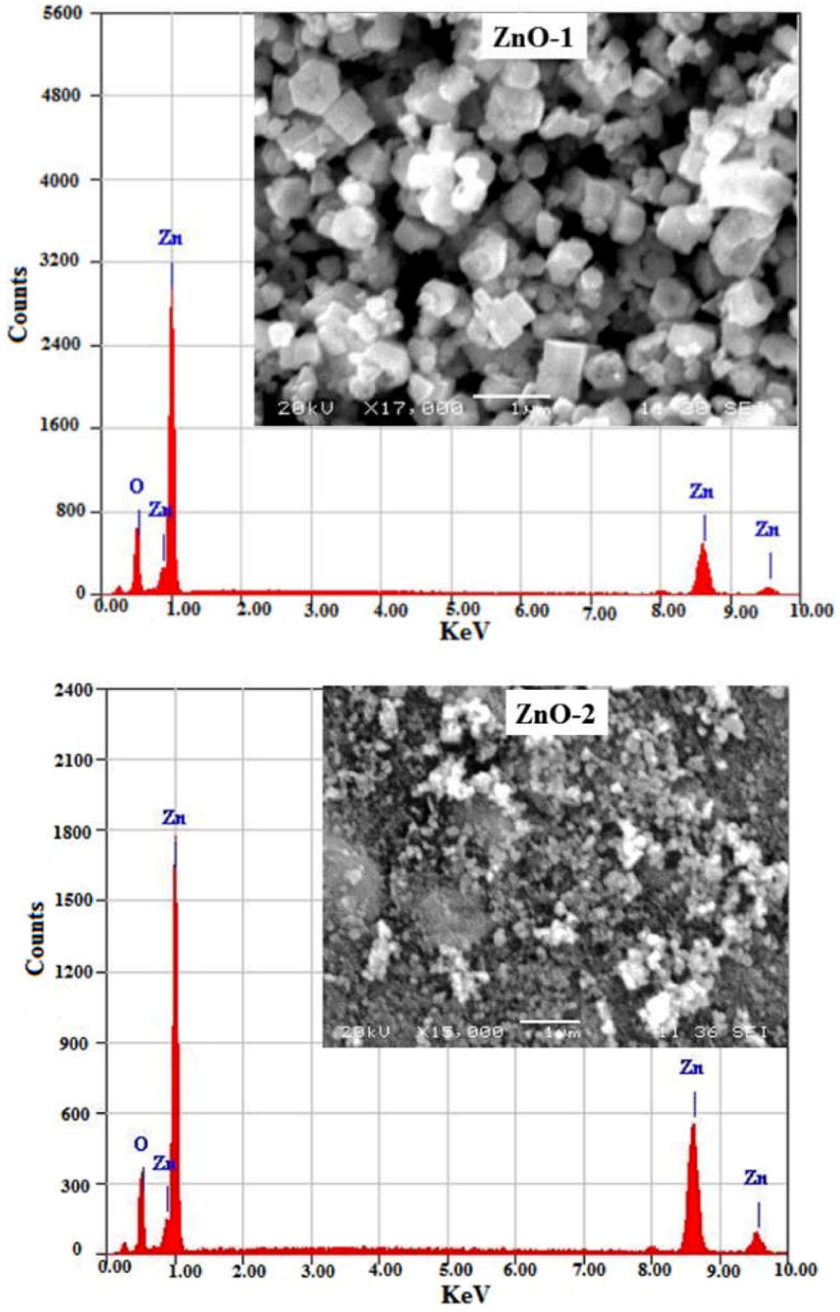

Figure 2. Scanning electron microscopy (SEM) and EDX images of ZnO-1 and ZnO-2 nanoparticles.

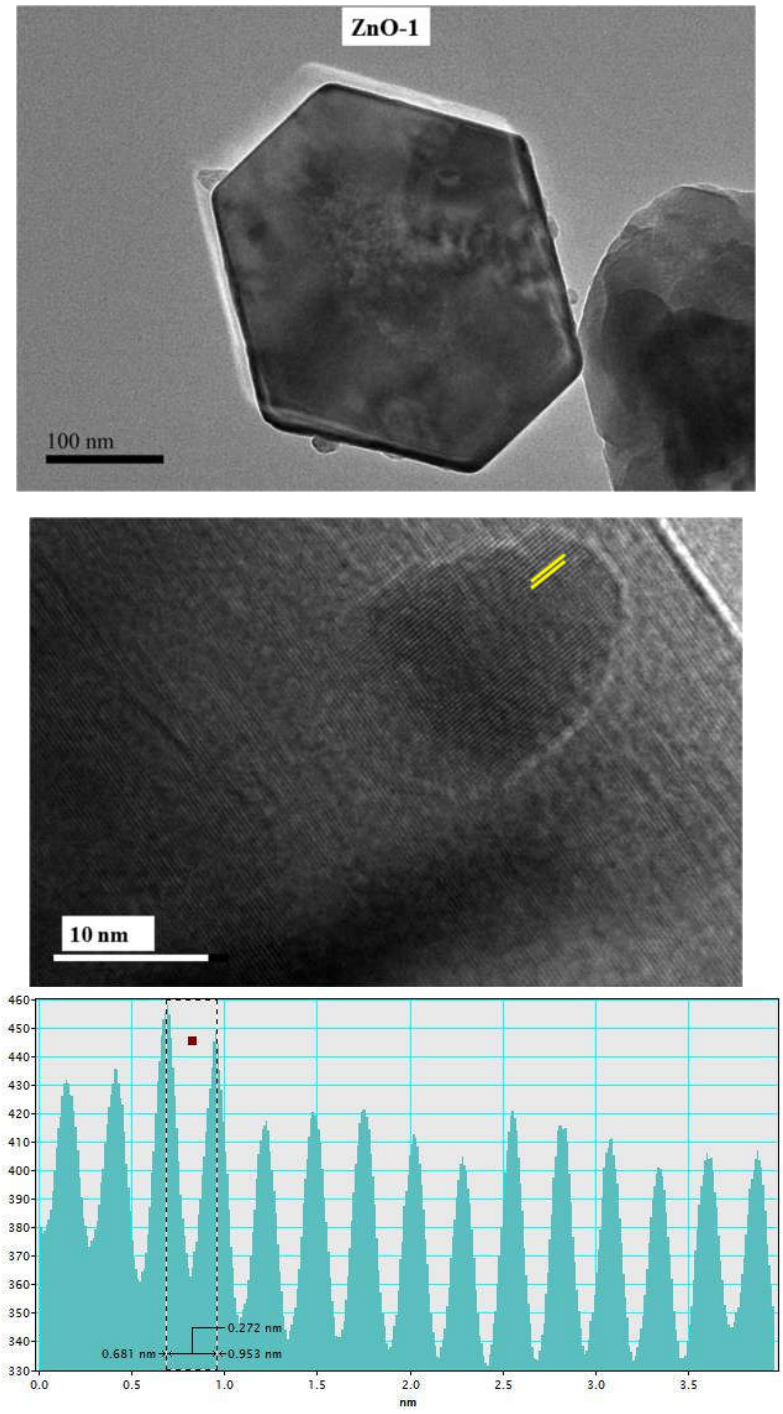
ZnO-1
100 nm
10 nm
460
450
440
430
420
410
400
390
380
370
360
350
340
330
0.272 nm
0.681 nm
0.953 nm
0.0
0.5
1.0
1.5
2.0
2.5
3.0
3.5
nm

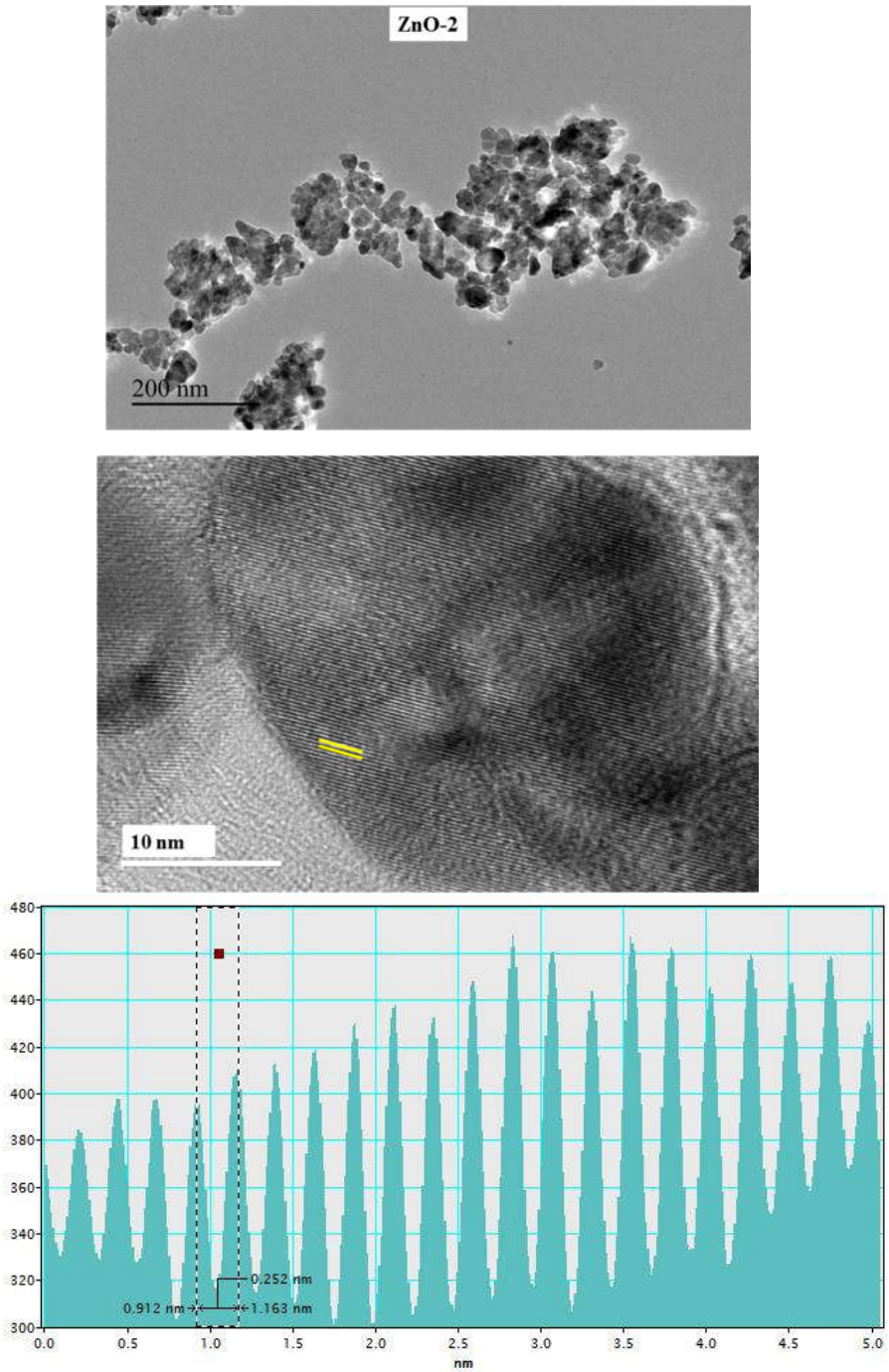

Figure 3. TEM and HRTEM images of ZnO-1 and ZnO-2 nanoparticles.

Fourier transform infra-red spectroscopy (FTIR) analysis

The FTIR spectra of the prepared ZnO nanoparticles are presented in Figure 4. The broadband obtained in the range of 3389-3422 cm^{-1} corresponds to the presence of hydrogen-bonded hydroxide (O-H) stretching mode of vibration from water to the ZnO nanoparticles. The Zn–O stretching mode of vibration shows bands in the range from 600 to 400 cm^{-1}; in consequence, the band at 473 and 481 cm^{-1} confirms the formation of ZnO nanoparticles [27, 29]. The bands obtained at 1591 cm^{-1} and 1398 cm^{-1} are associated with water molecules O–H bending modes [27, 29].

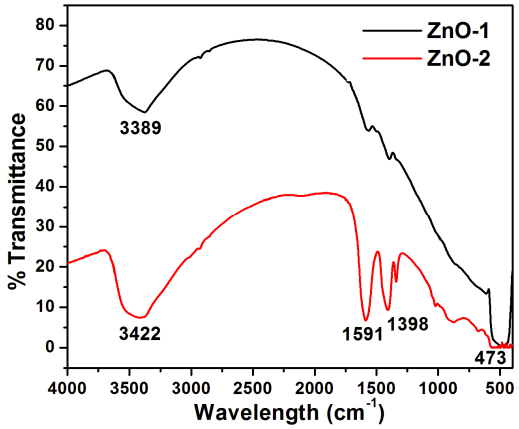

Figure 4. FTIR spectra of ZnO-1 and ZnO-2 nanoparticles.

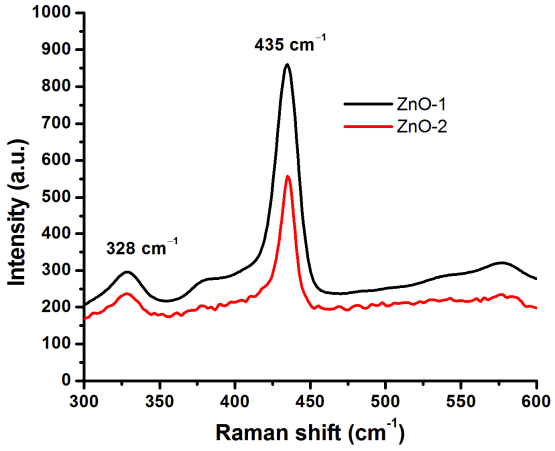

Figure 5. Raman spectra of ZnO-1 and ZnO-2 nanoparticles.

Raman analysis

The crystallinity and structural ailment in micro and nanostructured materials are studied by the Raman spectroscopy and shown in Figure 5. The space group of ZnO nanoparticles with hexagonal wurtzite structure is *P*63*mc.* As observed in Figure 5, two peaks are obtained at 435 cm^{-1} (strong) and 328 cm^{-1}. The peak at 435 cm^{-1} represented the E_2 (high) mode of Raman active,

which is a typical peak for the ZnO hexagonal wurtzite structure. The E_2 mode point toward high crystallinity and very low oxygen vacancy in ZnO nanoparticles. Peak 328 cm^{-1} represents to the E_{2H}–E_{2L} (multi-phonon process) mode, and it can form only a single-crystal ZnO [29-31]. No specific influence of stabilizing agent is perceived on the method of ZnO nanoparticles except peak intensity ratio. The reported results are in good agreement with the Raman spectrum of ZnO described by Yousefi *et al.* [32].

Optical properties

The UV-Vis spectra of ZnO-1 and ZnO-2 nanoparticles are shown in Figure 6. Strong absorption bands are obtained at 458 nm for ZnO-1 and 418 nm for ZnO-2 nanoparticles, which are associated with the absorption bands of ZnO. Further, the nature of the optical band gap will be preserved when the absorption spectrum moves to longer wavelengths along with the electron excitation from the valance band to the conduction band. The following equation is used to calculate the optical band gap (Eg):

$(Ah\nu)^n = B(h\nu - Eg)$

where $h\nu$ is the photon energy; A represents absorbance, B represents constant linked to the material; and n refers to either 2 or ½ for direct and indirect transitions, respectively. Therefore, the optical band gap for the absorption peak is gained by extending the linear portion of the $(Ah\nu)^n$ -$h\nu$ curve to zero, as presented in Figure 6.

In literature, the band gap energy of the bulk ZnO is found to be 3.37 eV, but in the present work, the band gap of ZnO-1 and ZnO-2 nanoparticles are found to be 2.9 and 3.0 eV, which is smaller than that of the bulk ZnO. This might be due to the existence of hydroxyl group (-OH) adsorbed on the surface of ZnO nanoparticles which is evidenced by FTIR analysis and might reduce the band gap energy [33]. The band gap of materials is not significantly changed with diethylamine and triethylamine. On the other hand, the changes in their morphologies, particle size, and surface microstructures affect the redshift of the spectral lines, which will lead to better crystallinity [34-35]. In addition, it is found that the band gap of the transport layer has a crucial role in defining the performance of dye-sensitized solar cells [36].

Table 1. Photovoltaic performance of ZnO-1 based device with (a) dye-1, (b) dye-2 and (c) dye-3.

Dye	V_{oc} (V)	J_{sc} (mA/cm^2)	Fill factor (ff)	η Efficiency (%)
dye-1	0.31	1.709	0.59	0.73
dye-2	0.41	1.647	0.58	0.90
dye-3	0.45	2.128	0.66	1.45

Photovoltaic performance

Figure 7 shows the J-V curves of DSSC prepared by ZnO-1 nanoparticle to see their applicability. We selected the ZnO-1 nanoparticle due to the porosity and wide-band gap. We also tried with ZnO-2, but unfortunately, the results were inappropriate; therefore, we did not mention it in the current report. The short-circuit density (J_{sc}), the open-circuit voltage (V_{oc}), and the fill factor (FF) parameters for the solar cells are measured and shown in Table 1. The best photovoltaic performance of the ZnO-1 was obtained with dye 3 with PCE of 1.45%, the open-circuit voltage of 0.454 V, short-circuit current density of 2.128 mA/cm^2, and 0.66 fill factor. This enhancement in efficiency has been attributed to the small energy band gap of dye-3 and better energy alignment with ZnO-1 nanoparticles, which could provide better charge transport. The achieved photovoltaic parameters are précised in Table 1. The results obtained from the current study are lower than the efficiencies reported in the literature. Keis *et al.* [37] reported that ZnO nanoparticle film with N719 dye showed 5% efficiency, whereas Chang *et al.* [38] reported 5.6% efficiencies with

similar properties. As far as nano wire-based DSSCs are concerned, Law *et al.* [19] reported up to 1.5% efficiency, but Xu *et al.* [39] have attained 2.1% efficiency by optimized ZnO NWs with a length of up to 30 µm. Even though some DSSCs based on ZnO showed lower efficiencies than those stated in the current study. The reasons behind the low efficiency or performance of ZnO-based DSSCs are not exclusively implicit. But, the nanoparticles of larger size and narrow optical band gap were found less suitable for dye loading. They increased the charge recombination as they could not provide continuous pathways to the electrons. On the other hand, the decrease in the photocurrent efficiency of dye-1 and dye-2 sensitized devices is attributed to the blue-shifted dyes with a greater energy band gap than the ones of the dye-3.

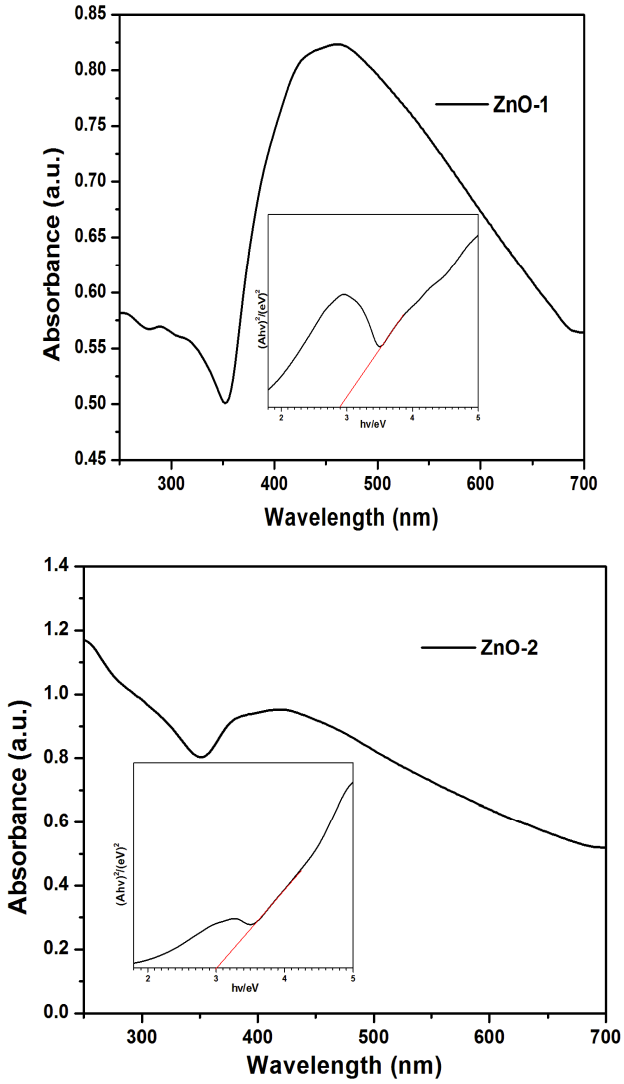

Figure 6. The UV-Vis spectra and optical band gap of ZnO-1 and ZnO-2 nanoparticles.

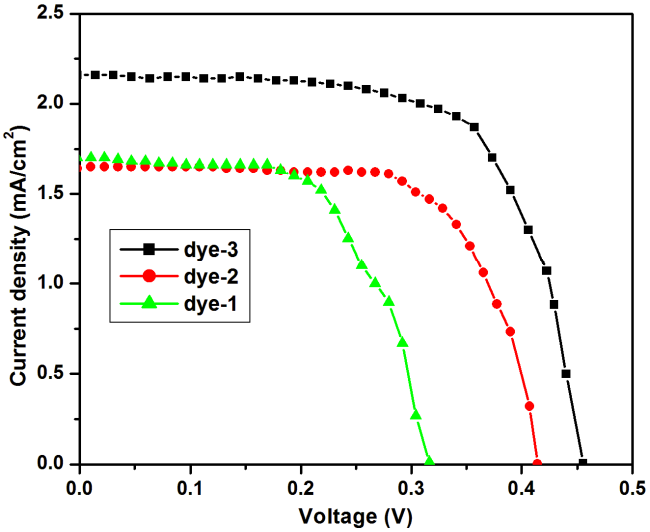

Figure 7. The current-voltage curve of ZnO-1 based device with (a) dye-1, (b) dye-2 and (c) dye-3.

CONCLUSION

The modified solvothermal method has been used to synthesize different morphologies of ZnO nanomaterials. The different morphologies and optical band gap were obtained for the ZnO by different stabilizers used in the synthesis. The band gap energy of ZnO-1 and ZnO-2 nanomaterials was 2.9 and 3.0 eV, which is smaller than that of the bulk ZnO. XRD patterns of all ZnO samples confirm the formation of a pure crystalline hexagonal phase. The photovoltaic performance of devices fabricated using ZnO-1, and dye-3 shows the highest efficiency. The difference in efficiencies with dye-1, dye-2, and dye-3 is due to their energy band gap. From the present study, we can transform the shape, size, and morphology of ZnO by changing the stabilizer and progress its performance as photoanode material in DSSCs.

ACKNOWLEDGMENT

The authors are very thankful to the Dean of Scientific Research, King Khalid University, Abha, Saudi Arabia for the funding under grant number RGP 2/188/43.

REFERENCES

1. Ozgur, U.; Alivov, Y.I.; Liu, C.; Teke, A.; Reshchikov, M.A.; Dogan, S.; Avrutin, V.; Cho, S.J.; Morkoc, H. A comprehensive review of ZnO materials and devices. *J. Appl. Phys.* **2005**, 98, 041301.
2. Li, L.; Zhai, T.; Bando, Y.; Golberg, D. Recent progress of one-dimensional ZnO nanostructured solar cells. *Nano Energy* **2012**, 1, 91-106.
3. Zhang, F.; Li, X.; Gao, X.; Wu, L.; Zhuge, F.; Wang, Q.; He, Y. Effect of defect content on the unipolar resistive switching characteristics of ZnO thin film memory devices. *Solid State Commun.* **2012**, 152, 1630-1634.

4. Cheng, X.L.; Zhao, H.; Huo, L.H.; Gao, S.; Zhao, J.G. ZnO nanoparticulate thin film: Preparation, characterization and gas-sensing property. *Sens. Actuators B chem.* **2004**, 102, 248-252.
5. Abo-El-Enein, S.A.; El-Hosiny, F.I.; El-Gamal, S.M.A.; Amin, M.S.; Ramadan, M. Gamma radiation shielding, fire resistance and physicochemical characteristics of Portland cement pastes modified with synthesized Fe_2O_3 and ZnO nanoparticles. *Constr. Build. Mater.* **2018**, 173, 687-706.
6. Dhodamani, A.G.; More, K.V.; Mullani, S.B.; Deshmukh, S.P.; Koli, V.B.; Panda, D.K; Delekar, S.D. Structural refinement and optoelectronic properties of $(Mo_xTi_{1-2x}O_{2-\delta})_{1-y}(RGO)_y$ nanocomposites and their photovoltaic studies with natural pigments as sensitizers. *Chem. Select* **2020**, 5, 218-230.
7. Delekar, S.D.; Dhodamani, A.G.; More, K.V.; Dongale, T.D.; Kamat, R.K.; Acquah, S.F.; Dalal, N.S.; Panda, D.K. Structural and optical properties of nanocrystalline TiO_2 with multiwalled carbon nanotubes and its photovoltaic studies using Ru(II) sensitizers. *ACS Omega* **2018**, 3, 3, 2743-2756
8. Dhodamani, A.G.; More, K.V.; Patil, S.M.; Shelke, A.R.; Shinde, S.K.; Kim, D.Y.; Delekar, S.D. Synergistics of Cr(III) doping in TiO_2/MWCNTs nanocomposites: Their enhanced physicochemical properties in relation to photovoltaic studies. *Solar Energy* **2020**, 201, 398-408.
9. Dhodamani, A.G.; More, K.V.; Koli, V.B.; Shelke, A.R; Deshpande, N.G.; Panda, D.K.; Delekar, S.D. Compositional dependent physicochemical and photovoltaic properties of the $(TiO_2)_{1-x}(RGO)_x$ nanocomposites for sensitized solar cells using Ru(II) dyes. *Chem. Select* **2019**, 4, 1055-1068.
10. Mathew, S.; Yella, A.; Gao, P.; Humphry-Baker, R.; Curchod-Basile, F.E.; Ashari-Astani, N.; Tavernelli, I.; Rothlisberger, U.; Nazeeruddin, K.; Grätzel, M. Dye-sensitized solar cells with 13% efficiency achieved through the molecular engineering of porphyrin sensitizers. *Nat. Chem.* **2014**, 6, 242-247.
11. Alwin, S.; Shajan, X.S. Facile synthesis of 3-D nanostructured zinc oxide aerogel and its application as photoanode material for dye-sensitized solar cells. *Surf. Interfaces* **2017**, 7, 14-19.
12. Sima, C.; Grigoriu, C.; Toma, O.; Antohe, S. Study of dye-sensitized solar cells based on ZnO photoelectrodes deposited by laser ablation and doctor blade methods. *Thin Solid Films* **2015**, 597, 206-211.
13. Aldeen, T.S.; Mohamed, H.E.A.; Maaza, M. ZnO nanoparticles prepared via a green synthesis approach: Physical properties, photocatalytic and antibacterial activity. *J. Phys. Chem. Solids* **2022**, 160, 110313.
14. Kotresh, M.G.; Patil, M.K.; Inamdar, S.R. Reaction temperature based synthesis of ZnO nanoparticles using co-precipitation method: Detailed structural and optical characterization. *Optik* **2021**, 243, 167506.
15. Vázquez, A.; López, I.A.; Gómez, I. Growth mechanism of one-dimensional zinc sulfide nanostructures through electrophoretic deposition. *J. Mater. Sci.* **2013**, 48, 2701-2704.
16. Adedokun, O.; Bello, I.T.; Sanusi, Y.K.; Awodugba, A.O. Effect of precipitating agents on the performance of ZnO nanoparticles based photo-anodes in dye-sensitized solar cells. *Surf. Interfaces* **2020**, 21, 100656-100663.
17. Samaneh, G.; Mohammad, A.; Mohammad, I. Simple mass production of zinc oxide nanostructures via low-temperature hydrothermal synthesis. *Mater. Res. Express* **2017**, 4, 035010.
18. Xu, L.; Hu, Y.-L.; Pelligra, C.; Chen, C.-H.; Jin, L.; Huang, H.; Sithambaram, S.; Aindow, M.; Joesten, R.; Suib, S. L. ZnO with different morphologies synthesized by solvothermal methods for enhanced photocatalytic activity. *Chem. Mater.* **2009**, 21, 2875-2885.

19. Law, M.; Greene, L.E.; Johnson, J.C.; Saykally, R.; Yang, P. Nanowire dye-sensitized solar cells. *Nat. Mater.* **2005**, 4, 455.
20. Law, M.; Greene, L.E.; Radenovic, A.; Kuykendall, T.; Liphardt, J.; Yang, P. ZnO−Al_2O_3 and ZnO−TiO_2 core-shell nanowire dye-sensitized solar cells. *J. Phys. Chem.* B **2006**, 110, 22652-22663.
21. Suh, D.I.; Lee, S.Y.; Kim, T.H.; Chun, J.M.; Suh, E.K.; Yang, O.B.; Lee, S.K. The fabrication and characterization of dye-sensitized solar cells with a branched structure of ZnO nanowires. *Chem. Phys. Lett.* **2007**, 442, 348-353.
22. Baxter, J.B.; Aydil, E.S. Dye-sensitized solar cells based on semiconductor morphologies with ZnO nanowires. *Sol. Energy Mater. Sol. Cells* **2006**, 90, 607-622.
23. Jiang, C.Y.; Sun, X.W.; Lo, G.Q.; Kwong, D.L.; Wang, J.X. Improved dye-sensitized solar cells with a ZnO-nanoflower photoanode. *Appl. Phys. Lett.* **2007**, 90, 263501.
24. Li, J.; Sang, X.; Chen, W.; Qin, C.; Wang, S.; Su, Z.; Wang, E. The application of ZnO nanoparticles containing polyoxometalates in dye-sensitized solar cells. *Eur. J. Inorg. Chem.* **2013**, 2013, 1951-1959.
25. Memarian, N.; Concina, I.; Braga, A.; Rozati, S.M., Vomiero, A.; Sberveglieri, G. Hierarchically assembled ZnO nanocrystallites for high-efficiency dye-sensitized solar cells. *Angew. Chem. Int. Ed. Engl.* **2011**, 50, 12321-12325.
26. Al-Sehemi, A.G.; Allami, S.A.S.; Kalam, A. Design and synthesis of organic dyes with various donor groups: promising dyes for dye-sensitized solar cells. *Bull. Mater. Sci.* **2020**, 43, 224-233.
27. Dinesh, V.P.; Biji, P.; Ashok, A.; Dhara, S.K.; Kamaruddin, M.; Tyagi, A.K., Raj, B. Plasmon-mediated highly enhanced photocatalytic degradation of industrial textile effluent dyes using hybrid ZnO@Ag core-shell nanorods. *RSC Adv.* **2014**, 4, 58930-58940.
28. Yoshida, T.; Terada, K.; Schlettwein, D.; Oekermann, T.; Sugiura, T.; Minoura, H. Electrochemical self-assembly of nanoporous ZnO/Eosin Y thin films and their sensitized photoelectrochemical performance. *Adv. Mater.* **2000**, 12, 1214-1217.
29. Kutty, R.G.; Seery, M.K.; Pillai, S.C. A highly efficient Ag-ZnO photocatalyst: Synthesis, properties, and mechanism. *J. Phys. Chem.* C **2008**, 112, 13563-13570**.**
30. Umar, A.; Hahn, Y.B. Aligned hexagonal coaxial-shaped ZnO nanocolumns on steel alloy by thermal evaporation. *Appl. Phys. Lett.* **2006**, 88, 173120.
31. Wu, J.J.; Liu, S.C. Catalyst-free growth and characterization of ZnO nanorods. *J. Phys. Chem.* B **2002**, 106, 9546-9551.
32. Yousefi, R.; Jamali-Sheini, F.; Cheraghizade, M.N; Khosravi-Gandomani, S.; Sáaedi, A.; Huang, N.M.; Basirun, W.J.; Azarang, M. Enhanced visible-light photocatalytic activity of strontium-doped zinc oxide nanoparticles. *Mater. Sci. Semicond. Process.* **2015**, 32, 152-159.
33. Subalakshmi, K.; Senthilselvan, J.; Kumar, K.A.; Kumar, S.A.; Pandurangan, A. Solvothermal synthesis of hexagonal pyramidal and bifrustum shaped ZnO nanocrystals: Natural betacyanin dye and organic Eosin Y dye-sensitized DSSC efficiency, electron transport, recombination dynamics, and solar photodegradation investigations. *J. Mater. Sci. Mater. Electron.* **2017**, 28, 15565-15595.
34. Babikier, M.; Wang, D.; Wang, J.; Li, Q.; Sun, J.; Yan, Y.; Jiao, S. Cu-doped ZnO nanorod arrays: the effects of copper precursor and concentration. *Nanoscale Res. Lett.* **2014**, 9, 199.
35. Ungula, J.; Dejene, B.F.; Swart, H.C. Effect of annealing on the structural, morphological and optical properties of Ga-doped ZnO nanoparticles by reflux precipitation method. *Results Phys.* **2017**, 7, 2022-2027.
36. Dubey, R.S.; Jadkar, S.R.; Bhorde, A.B. Synthesis, and characterization of various doped TiO_2 nanocrystals for dye-sensitized solar cells. *ACS Omega* **2021**, 6, 3470-3482.
37. Keis, K.; Magnusson, E.; Lindström, H.; Lindquist, S.; Hagfeldt, A. A 5% efficient photoelectrochemical solar cell based on nanostructured ZnO electrodes. *Sol. Energy Mater. Sol. Cells* **2002**, 73, 51-58.

38. Chang, W.; Lee, C.; Yu, W.; Lin, C. Optimization of dye adsorption time and film thickness for efficient ZnO dye-sensitized solar cells with high at-rest stability. *Nanoscale Res. Lett.* **2012**, 7, 688.
39. Xu, C.K.; Shin, P.; Cao, L.L.; Gao, D. Preferential growth of long ZnO nanowire array and its application in dye-sensitized solar cells. *J. Phys. Chem.* C **2010**, 114, 125-129.